Remote Sensing of Environment 128 (2013) 259–267

Contents lists available at SciVerse ScienceDirect

Remote Sensing of Environment

journal homepage: www.elsevier.com/locate/rse

An algorithm to retrieve absorption coefficient of chromophoric dissolved organic matter from ocean color

Qiang Dong [a], Shaoling Shang [a,b,*], Zhongping Lee [c]

[a] Research and Development Center for Ocean Observation Technologies, Xiamen University, Xiamen 361005, China
[b] State Key Laboratory of Marine Environmental Science, Xiamen University, Xiamen 361005, Fujian, China
[c] Environmental, Earth, and Ocean Sciences, University of Massachusetts at Boston, MA 02125, USA

ARTICLE INFO

Article history:
Received 4 July 2012
Received in revised form 18 September 2012
Accepted 15 October 2012
Available online xxxx

Keywords:
Chromophoric dissolved organic matter
Absorption coefficient
Algorithm
Quasi-analytical algorithm
Remote sensing

ABSTRACT

We extended the quasi-analytical algorithm (QAA) architecture to analytically derive absorption coefficient of chromophoric dissolved organic matter (a_g). Specifically, we used an empirical formula based on total absorption and particle backscattering coefficients to estimate and then remove detritus absorption coefficient (a_d), and developed a scheme to use absorption coefficients at three wavelengths (412, 443, and 490 nm) for the separation of a_g and a_{ph} (absorption coefficient of phytoplankton). The algorithm was tested using an in situ data set collected in the South China Sea and the Taiwan Strait and a global in situ data set—the NASA Bio-Optical Marine Algorithm Data set (NOMAD). Our results indicated that this new analytical algorithm for retrieving a_g performed reasonably well with a mean absolute percentage error of approximately 45% for $a_g(412)$, while it also presented a satisfactory performance for a_{ph} and a_d in both coastal and oceanic waters. Furthermore, the applicability of this new algorithm for general oceanographic studies was briefly illustrated by applying it to MODIS measurements over the Taiwan Strait and the shelf region near the Mississippi River delta. Nevertheless, more independent tests with in situ and satellite data are needed to further validate and improve this innovative approach.

1. Introduction

Gelbstoff, or chromophoric dissolved organic matter (CDOM; frequently used abbreviations are summarized in Table 1), is an optically active component and plays an important role in carbon cycling (Coble, 2007). CDOM provides an effective sun shade, modulates the underwater light field and thus affects the growth of phytoplankton and other aquatic organisms (e.g., Jerlov, 1968; Karentz & Lutze, 1990). In addition, CDOM makes up part of the pool of dissolved organic carbon (e.g., Nelson et al., 1998; Vodacek et al., 1997). It is important therefore to study CDOM, including its abundance, source, composition, and final fate at local and global scales, in order to eventually model and forecast CDOM's variations as well as its contributions to global carbon budgets (e.g., Mannino et al., 2008).

Because field studies, although quite precise and extremely useful, provide limited information in space and time, CDOM property obtained through satellite remote sensing is the only feasible means to inform its distribution at global scales. In the past decades, semi-analytical algorithms to retrieve the absorption coefficients of the sum (a_{dg}; m^{-1}) of CDOM (a_g; m^{-1}) and detritus (a_d; m^{-1}), collectively named as CDM, have been developed (Carder et al., 1999; IOCCG, 2006), enabling the characterization of CDM on a global scale (e.g., Siegel et al., 2002). These algorithms, however, do not divide a_{dg} into a_g and a_d analytically, thus could not provide a precise evaluation for the spatial and temporal variations of a_g, a proxy for CDOM. Recently, Mannino et al. (2008) developed an empirical algorithm to retrieve a_g for coastal waters in the middle Atlantic Bight, but it is not clear if the empirical coefficients are applicable to other regions or oceanic waters. Separately, Zhu et al. (2011) used data measured in the Mississippi River plume to develop a semi-analytical algorithm for the separation of a_g from a_{dg} and achieved some successes for their data set. The derivation of a_d there followed the approach of Lee (1994), i.e., using derived particle backscattering coefficient (b_{bp}; m^{-1}) as an input to estimate a_d. Our latest in situ measurements suggest that this approach may be reasonable for turbid coastal waters where suspended particles are dominated by mineral particles (e.g., Mississippi River plume), but may have limitations for waters where particles are dominated by phytoplankton (e.g., oceanic waters). Therefore, for the evaluation of CDOM in both coastal and oceanic waters, there is still a lack of robust algorithm to estimate a_g from ocean color satellite measurements.

Here, we propose a new approach to derive CDOM absorption coefficient from ocean color based on the quasi-analytical algorithm (QAA; Lee et al., 2002). The performance of the approach is assessed using an in situ data set collected in the South China Sea and the Taiwan Strait (hereafter abbreviated as SCSD) and a global scale in

* Corresponding author at: Research and Development Center for Ocean Observation Technologies, Xiamen University, Xiamen 361005, China. Tel./fax: +86 592 2184781.
E-mail addresses: slshang@gmail.com, slshang@xmu.edu.cn (S. Shang).

0034-4257/$ – see front matter © 2012 Elsevier Inc. All rights reserved.
http://dx.doi.org/10.1016/j.rse.2012.10.013

Table 1
Symbols, abbreviations and definitions.

Symbol	Description	Unit
a_d	Absorption coefficient of detritus	m^{-1}
a_{dg}	Absorption coefficient of detritus and CDOM	m^{-1}
a_g	Absorption coefficient of CDOM	m^{-1}
a_p	Particulate absorption coefficient ($a_p = a_{ph} + a_d$)	m^{-1}
a_{ph}	Absorption coefficient of phytoplankton	m^{-1}
a_{phg}	Absorption coefficient of phytoplankton and CDOM	m^{-1}
a_{nw}	Total absorption coefficient without pure water contribution ($a_{nw} = a_{ph} + a_d + a_g$)	m^{-1}
b_{bp}	Backscattering coefficient of suspended particles	m^{-1}
CDOM	Chromophoric dissolved organic matter	
NOMAD	NASA Bio-Optical Marine Algorithm Data set	
QAA	Quasi-analytical algorithm (Lee et al., 2002)	
R_{rs}	Above-surface remote-sensing reflectance	sr^{-1}
S_{ag}	Spectral slope for CDOM absorption coefficient	nm^{-1}
S_{ad}	Spectral slope for detritus absorption coefficient	nm^{-1}
SCSD	In situ data set collected in the South China Sea and the Taiwan Strait	

situ data set—the NASA Bio-Optical Marine Algorithm Data set (NOMAD; Werdell & Bailey, 2005). As comparison, the performance of an earlier empirical-style algorithm (Mannino et al., 2008) and a semi-analytical algorithm (Zhu et al., 2011) was also assessed using the same data sets. The proposed algorithm is further applied to Moderate Resolution Imaging Spectroradiometer (MODIS) measurements over the Taiwan Strait and the shelf region near the Mississippi River delta to briefly illustrate its applicability for general oceanographic studies.

2. Data and methods

2.1. SCSD data set

The SCSD data were collected during 10 cruises over the years of 2003–2007. They included five parameters, which were remote-sensing reflectance (R_{rs}; sr^{-1}), total absorption coefficient without water (a_{nw}; m^{-1}), a_g, a_d, and absorption coefficient of phytoplankton (a_{ph}; m^{-1}).

The above-surface R_{rs} was derived from the measurements of (1) upwelling radiance (L_u; $W\ m^{-2}\ nm^{-1}\ sr^{-1}$), (2) downwelling sky radiance (L_{sky}; $W\ m^{-2}\ nm^{-1}\ sr^{-1}$), and (3) radiance from a standard Spectralon reflectance plaque (L_{plaque}; $W\ m^{-2}\ nm^{-1}\ sr^{-1}$). The instrument used was the GER1500 spectroradiometer (Spectra Vista Corporation, USA), which covers a spectral range of 350–1050 nm with a spectral resolution of 3 nm. From these three components, R_{rs} can be calculated as:

$$R_{rs} = \rho \times \frac{L_u - F \times L_{sky}}{\pi \times L_{plaque}} - \Delta \quad (1)$$

where ρ is the reflectance of the Spectralon plaque with Lambertian characteristics, and F is the surface Fresnel reflectance (around 0.023 for the viewing geometry). $\Delta(sr^{-1})$ accounts for the residual surface contribution (glint, etc.), which was determined either by assuming $R_{rs}(750) = 0$ (clear oceanic waters) or through iterative derivation according to optical models for coastal turbid waters, as described in Lee et al. (2010).

Measurements of a_g were performed according to the Ocean Optics Protocols Version 2.0 (Mitchell et al., 2000), and were detailed in Hong et al. (2005) and Du et al. (2010). Briefly, seawater was filtered with a thoroughly cleaned 0.2-μm Millipore filter, and the absorbance of the filtered water was measured in a 10-cm quartz cell between 250 and 800 nm with 1 nm increment using a Varian Cary100 dual-beam spectrophotometer. The reference was 0.2-μm filtered MilliQ water. After converting the absorbance to absorption coefficient, a nonlinear least square regression (Eq. 2 with $\lambda_0 = 443$ nm) was employed to obtain the spectral slope (S_{ag}; nm^{-1}) over a wavelength range from 300 to 500 nm (Bricaud et al., 1981).

$$a_g(\lambda) = a_g(\lambda_0) \times \exp\left(-S_{ag}(\lambda - \lambda_0)\right) \quad (2)$$

The particulate absorption coefficient (a_p; m^{-1}) was measured by the filter-pad technique (Kiefer & Soohoo, 1982) with a dual-beam PE Lambda 950 spectrophotometer equipped with an integrating sphere (150 mm in diameter), in accordance with a modified Transmittance-Reflectance (T-R) method (Dong et al., 2008; Tassan & Ferrari, 1995). This approach was selected instead of the T method recommended in the NASA protocol (Mitchell et al., 2000), because some of the samples were rich in highly scattering non-pigmented particles; as a result, the standard T method overestimated the sample absorption (Dong et al., 2009; Tassan & Ferrari, 1995). Coefficient a_d was obtained by repeating the measurement on samples after pigment extraction by methanol (Kishino et al., 1985), and then a_{ph} was calculated by subtracting a_d from a_p. Eq. (3) with $\lambda_0 = 443$ was fitted by a nonlinear least square regression to obtain the spectral slope (S_{ad}; nm^{-1}) over a wavelength range from 400 to 600 nm.

$$a_d(\lambda) = a_d(\lambda_0) \times \exp(-S_{ad}(\lambda - \lambda_0)) \quad (3)$$

In total, there were 104 sets of in situ data, of which 86% was from the Taiwan Strait and the other 14% was from the South China Sea (see their locations in Fig. 1). The Taiwan Strait, a shallow channel connecting the South China Sea with the East China Sea, has complex hydrographic conditions determined by influences of several currents under the forcing of monsoonal winds (e.g., Jan et al., 2002). Several medium-sized rivers and numerous bays are located on the west coast (on mainland China) of the strait. Algae blooms often occur during spring in these bays (e.g., Wang et al., 2009). Also along this coast, upwelling develops in summer, driven by the prevailing southwest monsoon, which runs parallel to the coast due to Ekman transport (e.g., Hong et al., 2009). The Taiwan Strait portion of the SCSD mainly consisted of summer upwelling samples, intensive algae bloom samples in two bays (Xiamen Bay and Huangqi Bay), and samples in the vicinity of river mouths.

The South China Sea is one of the largest marginal seas in the world. Its basin is deep (~5000 m) and oligotrophic, with surface chlorophyll concentration lower than 0.1 mg/m^3 except in winter (e.g., Liu et al., 2002; Shang et al., 2012). Two large rivers, the Pearl River and the Meikong River, discharge into the South China Sea. Plume-induced blooms are often observed (e.g., Dai et al., 2008). Meso-scale eddies and upwelling events are also prominent, resulting in significant biological enhancements (e.g., Chen et al., 2007; Gan et al., 2009).

In summary, this in situ data set used for algorithm assessment covered a variety of coastal and oceanic water regimes, and thus a wide range of absorption properties, with $a_{nw}(443)$ ranging from 0.021 to 2.16 m^{-1}, and the ratios of $a_{ph}(443)/a_{nw}(443)$, $a_g(443)/a_{nw}(443)$, and $a_d(443)/a_{nw}(443)$ varying in a range of 8.9%–78.9%, 5.4%–54.8%, and 6.9%–85.7%, respectively.

2.2. NOMAD data set

The NOMAD data set was downloaded from the website: http://seabass.gsfc.nasa.gov/. This is a publicly available, global, in situ bio-optical data set for use in ocean color algorithm development and satellite data product validation activities (Werdell & Bailey, 2005). In this data set, 89 sets contain concurrent R_{rs}, a_{nw}, b_{bp} and a_d, which were used to derive empirical functions (see Eqs. 7–8 in

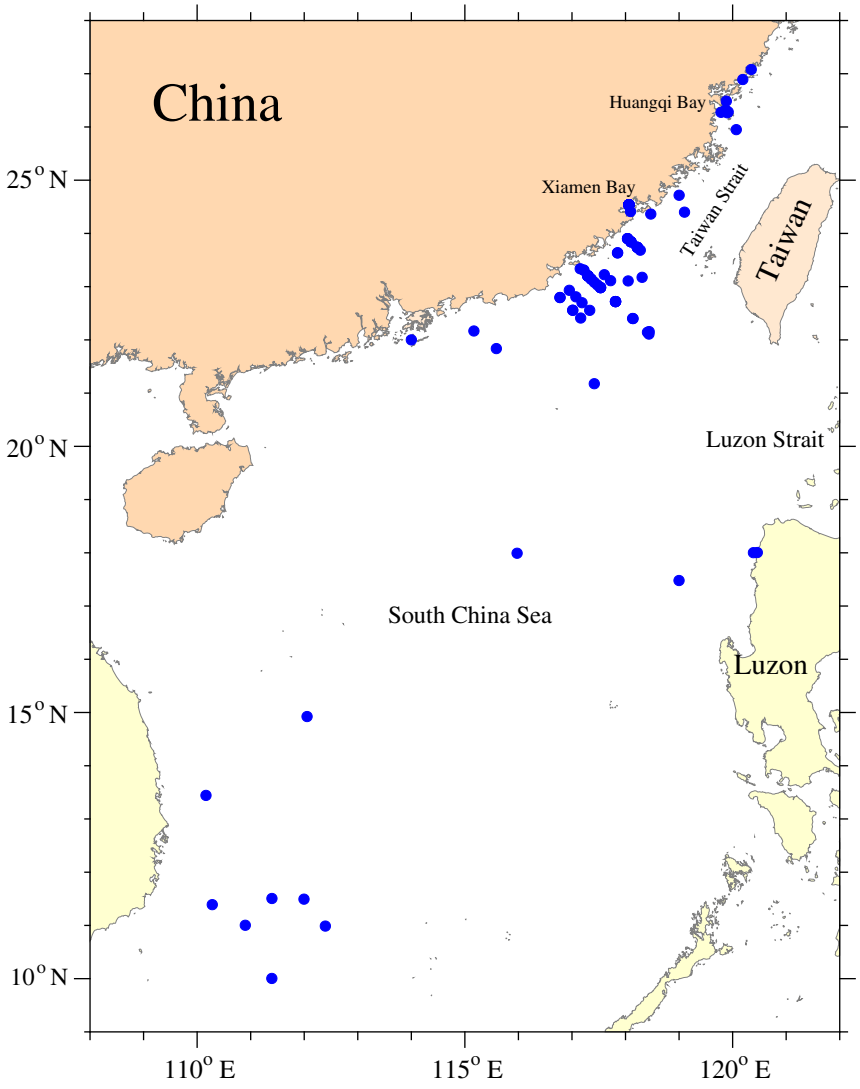

Fig. 1. Map of the South China Sea and the Taiwan Strait. Blue circles represent sampling stations where the match-up data set was collected.

Section 3.1), while the other 669 sets of R_{rs}, a_g, a_d and a_{ph} were used to evaluate the algorithm performance.

2.3. Error statistics

To evaluate algorithm performance, we used the determination coefficient (R^2), the mean absolute percentage error (ε), the bias (δ), and the root mean square error ($RMSE$) in log scale to describe the similarity/difference between the in situ data (x_i) and the retrieved data (y_i). These parameters are defined as follows:

$$\varepsilon = \frac{1}{n}\sum_{i=1}^{n}\frac{|y_i - x_i|}{x_i} \times 100\% \quad (4)$$

$$\delta = \frac{1}{n}\sum_{i=1}^{n}[\log_{10}(y_i) - \log_{10}(x_i)] \quad (5)$$

$$RMSE = \sqrt{\frac{1}{n}\sum_{i=1}^{n}[\log_{10}(y_i) - \log_{10}(x_i)]^2} \quad (6)$$

where n is the number of valid retrievals. All the calculations were guided, and the calculations were also guided by the need for a straightforward comparison with published results (e.g., IOCCG, 2006; Mélin et al., 2007).

3. Algorithm to partition a_d, a_g and a_{ph}

The QAA was developed by Lee et al. (2002) to derive the inherent optical properties of optically deep waters. Its inversion process is separated into two consecutive steps: the first derives a_{nw} and b_{bp}, and the second decomposes the derived a_{nw} into a_{ph} and a_{dg} using known properties at two wavelengths of 412 and 443 nm. Here we modify the second step to obtain a_g as well as a_d and a_{ph}. First, we removed a_d from a_{nw} by using an empirical formula based on the total absorption and the particle backscattering coefficients derived by QAA; then we retrieved a_g from a_{phg} (i.e., $a_{ph}+a_g$, which equals a_{nw}–a_d) by employing a_{phg} properties at three wavelengths of 412, 443, and 490 nm. The derivation procedures are listed in Table 2 and demonstrated by a schematic flow chart (Fig. 2).

3.1. Derivation of a_d

Because detritus is part of the suspended particulates and contributes to the scattering processes, various relationships between a_d and b_{bp} have been presented (Lee, 1994; Matsuoka et al., 2007; Tzortziou et al., 2007) and may be used to estimate a_d from b_{bp}.

Table 2
Steps of proposed algorithm for separations of a_d, a_g and a_{ph}.

Step	Property	Calculations
1	$a_{nw}(\lambda)$, $b_{bp}(\lambda)$	QAA(v5), (Lee et al., 2009)
2	a_d (443)	$a_d(443)=0.60\times\sigma^{0.90}, \sigma=0.05\times a_{nw}(443)+b_{bp}(555)\times 1.4^{\frac{R_{rs}(555)+R_{rs}(670)}{R_{rs}(443)}}$
3	a_d (λ)	$a_d(\lambda)=a_d(443)\times e^{-S_{ad}(\lambda-443)}, S_{ad}=0.012$
4	a_{phg} (λ)	$a_{phg}(\lambda)=a_{nw}(\lambda)-a_d(\lambda)$
5	a_g (443)	$a_g(443)=a_{phg}(443)/(1+9.56\times10^4\times e^{-11.13\times\psi})$ $\psi=\frac{a_{phg}(\lambda_2)}{a_{phg}(\lambda_0)}+\frac{a_{phg}(\lambda_1)-a_{phg}(\lambda_2)}{a_{phg}(\lambda_0)}\times\frac{\lambda_2-\lambda_0}{\lambda_2-\lambda_1}, \lambda_1=412, \lambda_0=443, \lambda_2=490$
6	a_g (λ)	$a_g(\lambda)=a_g(443)\times e^{-S_{og}(\lambda-443)}, \quad S_{ag}=0.0156+0.0164\times e^{-31.1\times a_g(443)}$
7	a_{ph} (λ)	$a_{ph}(\lambda)=a_{phg}(\lambda)-a_g(\lambda)$

Based on the 89 match-ups of $a_{nw}(443)$, $b_{bp}(555)$, R_{rs} and $a_d(443)$ in the NOMAD data set, an empirical relationship to estimate $a_d(443)$ was developed through trial and error ($R^2=0.56$, $RMSE=0.147$, Fig. 3):

$$a_d(443)=0.60\times\sigma^{0.90} \tag{7}$$

with σ as:

$$\sigma=0.05\times a_{nw}(443)+b_{bp}(555)\times 1.4^{\frac{R_{rs}(555)+R_{rs}(670)}{R_{rs}(443)}}. \tag{8}$$

Since $a_{nw}(443)$ and $b_{bp}(555)$ can be obtained by QAA, σ can be easily calculated; so can $a_d(443)$. Different from earlier approaches (Lee, 1994; Zhu et al., 2011), the above equations estimate a_d using three inputs. For coastal turbid waters, the ratio of $(R_{rs}(555)+R_{rs}(670))/R_{rs}(443)$ will be significantly greater than 1.0, then the $b_{bp}(555)$ component plays a bigger role for the estimation of a_d as indicated in earlier studies (Lee, 1994; Zhu et al., 2011). For oceanic waters, $(R_{rs}(555)+R_{rs}(670))/R_{rs}(443)$ could be significantly smaller than 1.0, then the $a_{nw}(443)$ component plays a bigger role for the $a_d(443)$ estimation (Morel, 2009). The combination of Eqs. (7)–(8) thus provides a seamless transition for the estimation of a_d of coastal and oceanic waters.

The a_d spectrum can then be calculated by Eq. (3) if S_{ad} is known. Various S_{ad} values have been reported and its range is relatively narrow (e.g., Roesler et al., 1989). For example, it has an average value of 0.011 nm^{-1} in the Irish Sea (Bowers et al., 1996), and of 0.0123 nm^{-1} in European coastal waters (Babin et al., 2003). In this study, we use the S_{ad} value of 0.012 nm^{-1}, which is an average value of S_{ad} in the Taiwan Strait (Dong, 2010).

3.2. Separation of a_g and a_{ph} in ocean color inversion

Once a_d is obtained, a_{phg} can be derived by subtracting a_d from a_{nw}:

$$a_{phg}(\lambda)=a_{nw}(\lambda)-a_d(\lambda). \tag{9}$$

In order to separate a_g from a_{phg}, we defined the parameter ψ as the ratio of the height of a straight line at 443 nm to the height of $a_{phg}(443)$ (i.e. BC/AC shown in Fig. 4a), where the straight line is determined between $a_{phg}(412)$ and $a_{phg}(490)$:

$$\psi=\frac{a_{phg}(\lambda_2)}{a_{phg}(\lambda_0)}+\frac{a_{phg}(\lambda_1)-a_{phg}(\lambda_2)}{a_{phg}(\lambda_0)}\times\frac{\lambda_2-\lambda_0}{\lambda_2-\lambda_1}, \lambda_1=412, \lambda_0=443, \lambda_2=490. \tag{10}$$

Because a_g and a_{ph} have different spectral characteristics, values of ψ vary with different combinations of a_g and a_{ph}. For instance, when a_{phg} has no contribution from a_{ph} (i.e., a_g alone), ψ will be greater than 1.0 (Fig. 4b). On the other hand, when a_{phg} has no contribution from a_g (i.e., a_{ph} alone), ψ will be less than 1.0 (Fig. 4c).

Based on an in situ data set collected in the Taiwan Strait, it is found that ψ has a good relationship with the ratio of $a_{ph}(443)/a_g(443)$ ($R^2=0.82$, $N=118$; Fig. 4d).

$$a_{ph}(443)/a_g(443)=9.56\times10^4\times e^{-11.13\times\psi} \tag{11}$$

Note that this data set was independent from the SCSD used for algorithm assessment, and the measurements of a_{ph} and a_g followed the same methods as described in Section 2. Therefore, with given $a_{phg}(443)$ and $a_{ph}(443)/a_g(443)$ ratio, $a_g(443)$ can be calculated,

$$a_g(443)=a_{phg}(443)/\left(1+9.56\times10^4\times e^{-11.13\times\psi}\right). \tag{12}$$

We tested this separation approach using the measured a_{phg} data (which are simply the sum of measured a_{ph} and a_g) in the NOMAD and SCSD data sets, and found that it performed very well (Fig. 5). The R^2 between calculated and measured properties is 0.97 and 0.91, with the *RMSE* of 0.200 and 0.228, for $a_{ph}(443)$ and $a_g(443)$, respectively, when the scheme was applied to the NOMAD data set. The results are 0.98, 0.87, with the *RMSE* of 0.135 and 0.203, respectively, for the SCSD data set. Because remote sensing platform does not obtain a_{phg} directly, the performance of the scheme is not expected to be as good as that applied to the in situ data set.

With $a_g(443)$ derived, the a_g spectrum can be calculated by Eq. (2) when S_{ag} is known. The S_{ag} values have a relatively broad range and

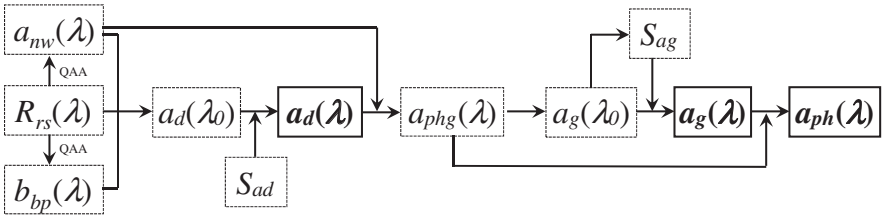

Fig. 2. Schematic flow chart of the proposed algorithm.

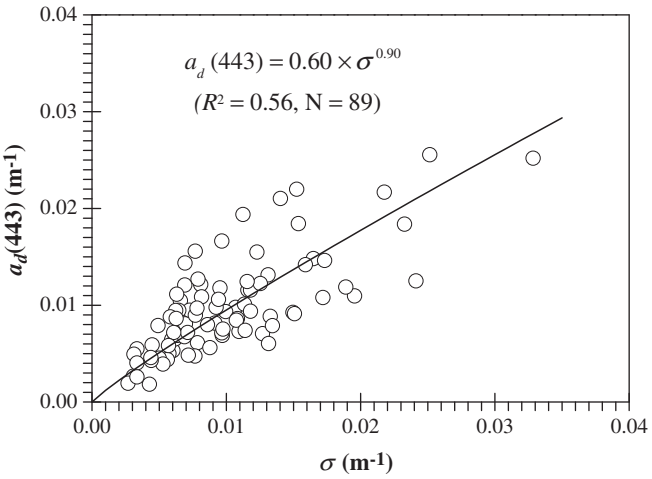

Fig. 3. Relationship between $a_d(443)$ and σ.

usually increase with a decrease in CDOM absorption (Blough & Vecchio, 2002; Green & Blough, 1994; Hong et al., 2005; Vodacek et al., 1997). In this study, S_{ag} was derived with an empirical formula as below, based on an in situ data set collected in the Taiwan Strait, which was not included in the SCSD (Dong, 2010).

$$S_{ag} = 0.0156 + 0.0164 \times e^{-31.1 \times a_g(443)} \quad (13)$$

Finally, a_{ph} spectrum is calculated by subtracting a_g from a_{phg}:

$$a_{ph}(\lambda) = a_{phg}(\lambda) - a_g(\lambda). \quad (14)$$

4. Evaluation of the algorithm

Measured R_{rs} in the SCSD and NOMAD was fed into the proposed algorithm to derive a_g as well as a_d and a_{ph}; the derived properties were then compared with measured properties. Results of the algorithm performance are shown in Table 3 and Fig. 6. The algorithms of Mannino et al. (2008) and Zhu et al. (2011) were tested using the same input as comparison and the results are also shown in Table 3.

While the derived $a_g(443)$ results show an underestimate as indicated by negative δ, the agreement between the derived and in situ $a_g(443)$ is rather satisfactory. Better performance was achieved for the SCSD ($R^2 = 0.68$, $\varepsilon = 45\%$, $RMSE = 0.253$) than for the NOMAD ($R^2 = 0.54$, $\varepsilon = 55\%$, $RMSE = 0.394$). Similar results were obtained for $a_{ph}(443)$ and $a_d(443)$. For example, for $a_{ph}(443)$, the values of R^2, ε and $RMSE$ for the SCSD are 0.81, 36% and 0.169, respectively, where the in situ $a_{ph}(443)$ is in the range of 0.008–1.613 m^{-1}. For the NOMAD data set with the $a_{ph}(443)$ range of 0.002–1.480 m^{-1}, these numbers are 0.63, 47% and 0.221, respectively. The less satisfactory results of the NOMAD data set might be due to larger uncertainties in the measured R_{rs}, where the measurement approaches were not uniform among various research groups, and consequently it was likely harder to achieve the same quality of the data. Separately, the fact of better performance for the SCSD might be partially due to the empirical function that separates a_g from a_{phg} (Eq. 11), which was derived from a regional data set collected in the Taiwan Strait. Although this regional data set was not included in the SCSD, they came from almost the same water, therefore bearing similar optical properties.

Compared to the algorithms of Mannino et al. (2008) and Zhu et al. (2011), our approach showed a better performance with the SCSD data set, for both a_g and a_d (Table 3). Similar ε and $RMSE$ values for a_g with the NOMAD data set were also found, except that our

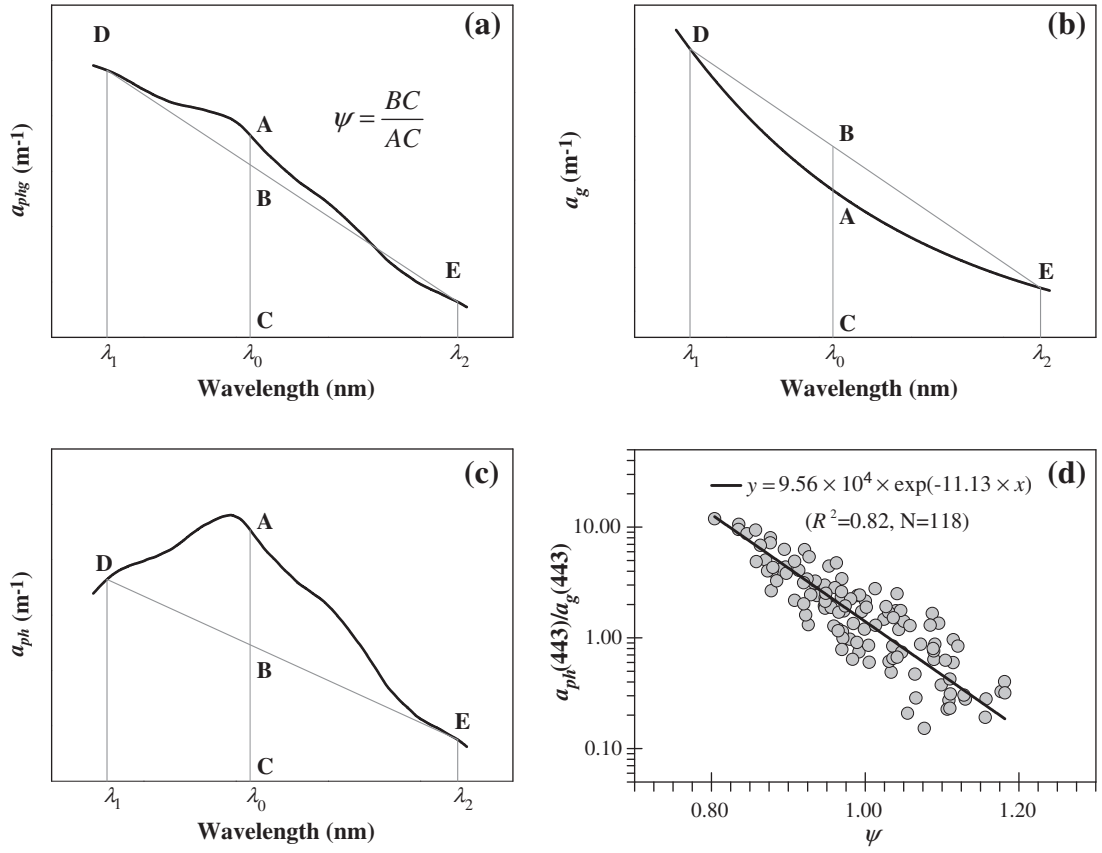

Fig. 4. (a) Sketch of ψ when a_{ph} and a_g both contribute to a_{phg}; (b) sketch of ψ when $a_{ph} = 0$; (c) sketch of ψ when $a_g = 0$. (d) Relationship between ψ and $a_{ph}(443)/a_g(443)$.

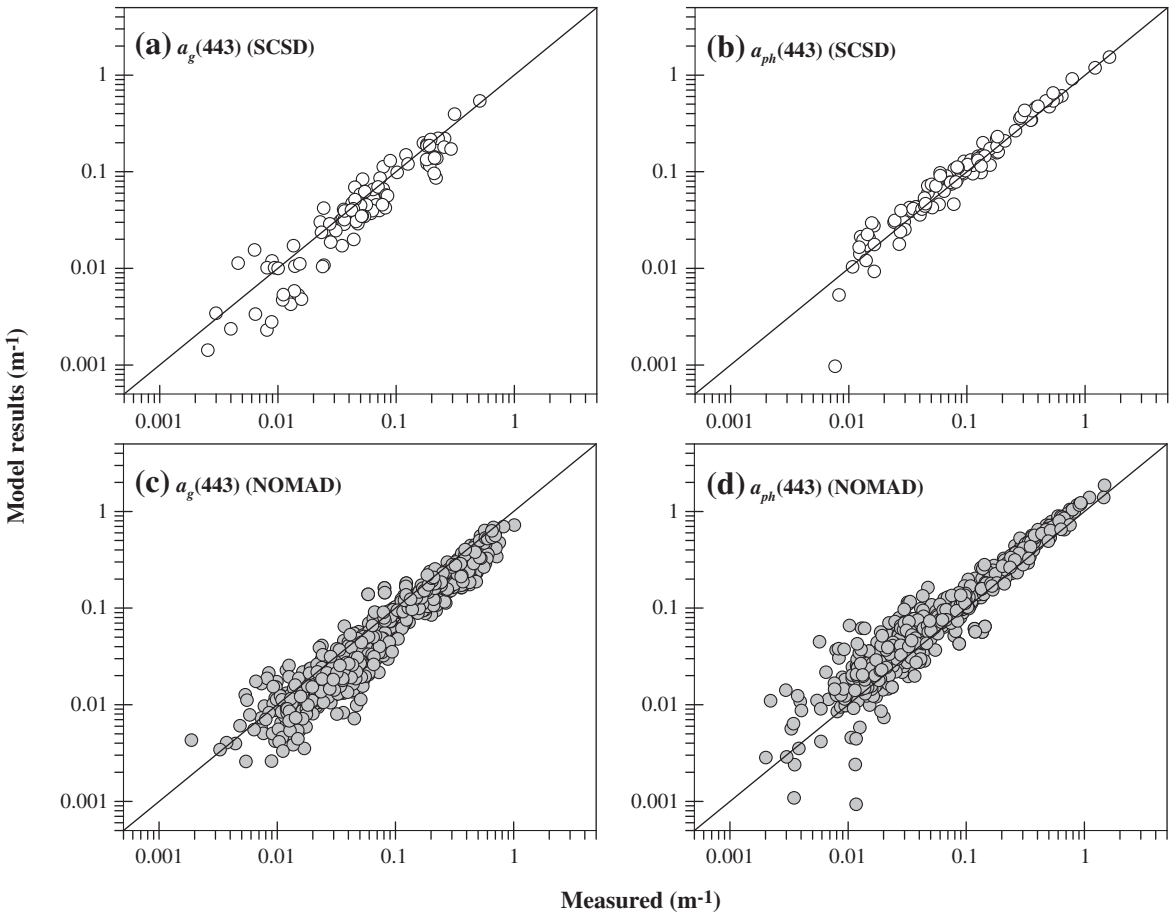

Fig. 5. (a and c) Measured a_g versus modeled a_g, which is partitioned from a_{phg} based on Eqs (10)–(13). (b and d) Measured a_{ph} versus modeled a_{ph} partitioned from a_{phg} using Eq. (14).

approach resulted in more serious underestimate of $a_g(443)$. However, we noticed that the $a_d(443)$ produced with the approach of Zhu et al. (2011) was deviated seriously from the observed $a_d(443)$, while ε and δ were 84% and −0.716, respectively. This indicates that using a combination of b_{bp}, a_{nw}, and R_{rs} to derive a_d, which was one of the key elements of the proposed algorithm in this study, was more adequate than the approaches that simply employ b_{bp} alone (Lee, 1994; Zhu et al., 2011). It is also noticeable that there were 172 invalid retrievals when using the empirical algorithm of Mannino et al. (2008). Of course, part of the less satisfied performance of the above two regional algorithms may be arisen from the fact that the empirical coefficients in the algorithms were not tuned using data included in this study.

The above results are encouraging because a_g, as an important biogeochemical property, is nearly analytically derived from ocean color measurements. This approach is likely applicable to global waters, although tests with more data are certainly needed.

Table 3
Error statistics between derived and in situ absorption coefficients.

	Band	R^2	ε (%)	*RMSE*	δ	*N*	*n*
SCSD data set							
a_g	412	0.67	40	0.222	−0.028	104	104
	443	**0.68**	**45**	**0.253**	−0.047	104	104
a_g^1	443	**0.24**	**74**	**0.327**	0.068	104	94
a_g^2	443	**0.33**	**155**	**0.414**	0.284	104	94
a_d	412	0.78	35	0.254	−0.136	104	104
	443	0.77	36	0.254	−0.148	104	104
a_d^1	443	0.66	69	0.704	−0.562	104	104
a_{ph}	412	0.71	32	0.171	0.016	104	104
	443	0.81	36	0.169	0.054	104	104
NOMAD data set							
a_g	412	0.55	45	0.315	−0.148	669	661
	443	0.54	55	**0.394**	**−0.203**	669	668
a_g^1	443	0.49	58	**0.315**	**−0.037**	669	649
a_g^2	443	0.63	57	**0.322**	**−0.095**	669	**497**
a_d	412	0.51	63	0.304	0.001	669	661
	443	0.47	63	0.308	−0.005	669	668
a_d^1	443	**0.02**	**84**	**0.878**	**−0.716**	669	667
a_{ph}	412	0.57	63	0.290	0.064	669	661
	443	0.63	47	0.221	0.049	669	668

N is the number of data tested, while n is the number of valid retrievals. a_g^1 and a_d^1 were derived using the approach of Zhu et al. (2011); a_g^2 was derived using the approach of Mannino et al. (2008).

5. Implications

Our results demonstrate that a_g can be analytically derived from remote sensing reflectance in both coastal and oceanic waters. This is especially significant for a better understanding of the biogeochemistry of coastal systems using satellite data. We previously reported seasonal variations of $a_g(412)$ based on field measurements in the near-shore waters of the Taiwan Strait (Du et al., 2010). In the present work, we produced climatological monthly mean $a_g(412)$ of this region using MODIS R_{rs} (version R2005.1, period of 2003–2008) as the input, based on the assumption that the default atmospheric correction approach (Gordon & Wang, 1994) was applicable to this region. The reason to produce climatological monthly mean numbers is that there were no applicable MODIS R_{rs} data during the cruise time (4–5 days) owing to serious influences of clouds and sun glints. To generate climatological monthly mean $a_g(412)$, daily $a_g(412)$ was first derived by feeding Level 2 daily R_{rs} of 1 km resolution (http://oceancolor.gsfc.nasa.gov/) into the proposed algorithm. Results in

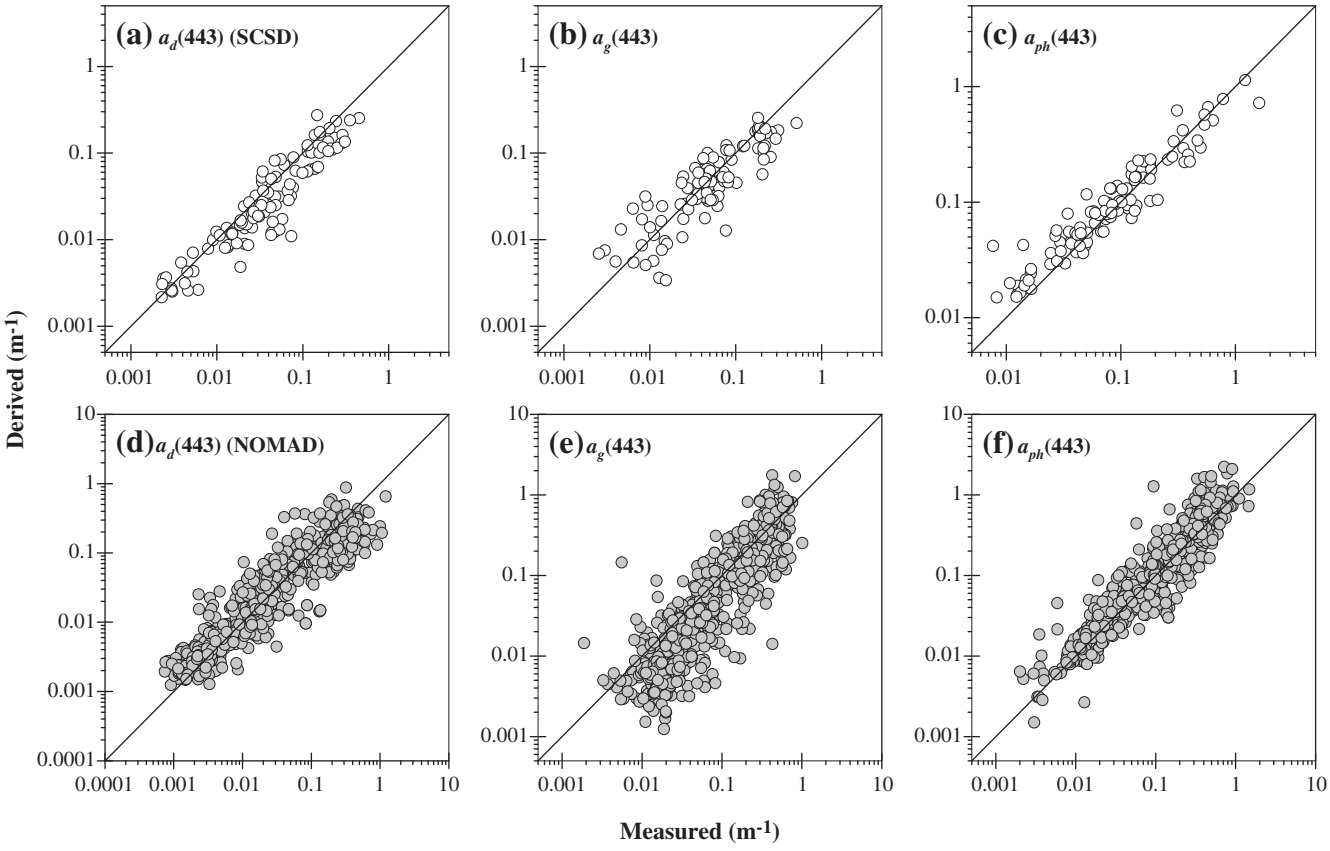

Fig. 6. Scatter plot showing the performance of the proposed ocean color inversion algorithm to retrieve absorption coefficients. (a–c): SCSD; (d–f): NOMAD.

April and October, corresponding to the months under in situ survey, are shown in Fig. 7. The mean $a_g(412)$ derived was found to be 0.159 and 0.203 m^{-1} in April and October, respectively, in the near-shore waters ($\leq$30 m) where the sampling stations were located. These remote sensing numbers are generally consistent with in situ results (0.123 ± 0.059 m^{-1} in April (wet season), 0.173 ± 0.036 m^{-1} in October (dry season)), and highlight the combined effects from ocean currents and river discharges on the CDOM distributions in the near-shore waters of the western Taiwan Strait.

Without separating a_g from a_{dg}, extra uncertainties will be lent to the estimation of salinity and the pressure of CO_2 (pCO_2) in the shelf waters under the influence of river input, if an a_g-based algorithm to estimate salinity and a salinity-based algorithm to estimate pCO_2 are used (Lohrenz & Cai, 2006). Fig. 8 shows the MODIS $a_g(412)$ and

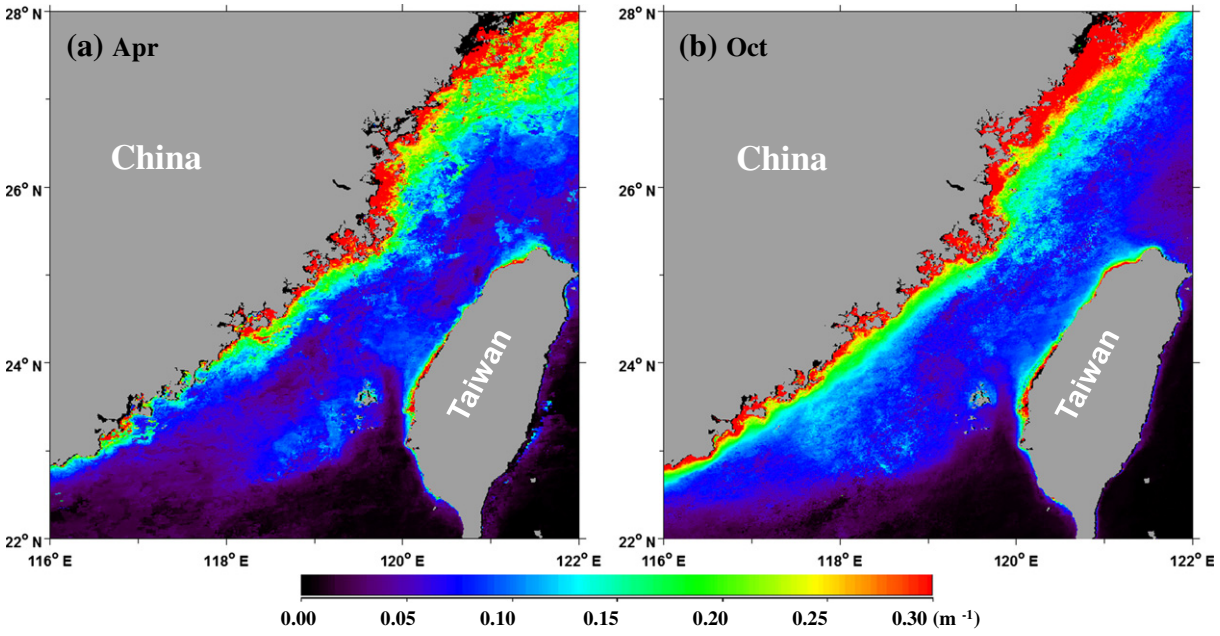

Fig. 7. Distribution of climatological monthly mean $a_g(412)$ in the Taiwan Strait derived from MODIS R_{rs} using the proposed inversion algorithm. (a) April; and (b) October.

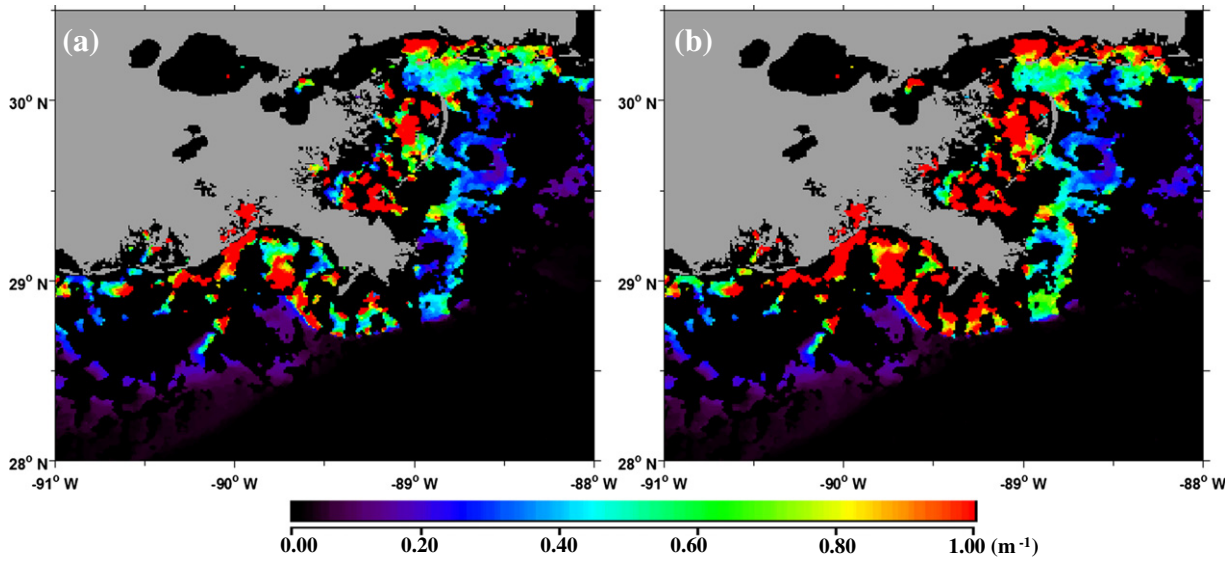

Fig. 8. Distributions of $a_g(412)$ (a) and $a_{dg}(412)$ (b) derived from MODIS R_{rs} using the proposed inversion algorithm on the shelf region near the Mississippi River delta on June 26, 2003.

$a_{dg}(412)$ in the shelf region near the Mississippi River delta on June 26, 2003, derived using our new approach. Evidently, $a_{dg}(412)$ could be two times greater than $a_g(412)$ in the near-shore waters where both detritus and CDOM were rich. In such waters, if $a_{dg}(412)$ is assumed the same as $a_g(412)$, salinity would be underestimated up to ~10 psu (Salinity $= -22.4 \times a_g(412) + 35.0$; Lohrenz & Cai, 2006). We postulate that this may be the main reason for a high positive bias in satellite estimates at low pCO_2 levels (RMSE = 72.8 μatm) observed by Lohrenz and Cai (2006).

6. Summary

Based on the general structure of the QAA scheme to retrieve inherent optical properties from remote sensing reflectance, we developed an innovative approach that uses absorption coefficients at three wavelengths (412, 443, and 490 nm) to analytically derive the absorption coefficient of CDOM. Encouraging results were achieved when the scheme was applied to two independent data sets (*RMSE* values were 0.222 and 0.315 for SCSD and NOMAD, respectively). We further applied the scheme to the MODIS measurements over the Taiwan Strait as well as the Mississippi River Delta, and found that the scheme not only generated consistent results compared with the in situ measurements but also improved the estimation of salinity in near-shore regions where absorption of CDOM is used as an input. While this new algorithm for retrieving CDOM absorption has produced encouraging results, as with all evaluations of remote sensing products (such as chlorophyll *a* concentration or diffuse attenuation coefficient), further studies and refinements are certainly required to ensure a robust application.

Acknowledgments

S. Shang was supported jointly by the NSF—China (# 40976068), the Chinese Ministry of Science and Technology through the National Basic Research Program (# 2009CB421201) and High-Tech R&D Program (# 2008AA09Z108). Q. Dong was supported by the Northern Gulf Institute (# NA06OAR4320264) while he was doing his postdoctoral research at the Mississippi State University. Z. Lee was partially supported by the Energy and Water Cycle Program of the National Aeronautics and Space Administration (# NNX09AV97G). We thank the crew of *R/V Yanping II*, and Jingyu Wu, Xiaoxin Ma, Xiaofei Sui, Wen Zhou, Wenqi Wang, Min Yang, Cuifen Du and Guomei Wei for their help in collecting the in situ data in the South China Sea and the Taiwan Strait. We are in debt to the NASA-OBPG, and data providers, for compiling and distributing NOMAD.

References

Babin, M., Stramski, D., Ferrari, G. M., Claustre, H., Bricaud, A., Obolensky, G., & Hoepffner, N. (2003). Variations in the light absorption coefficients of phytoplankton, non algal particles and dissolved organic matter in coastal waters around Europe. *Journal of Geophysical Research*, *108*, 3211–3231.

Blough, N. V., & Vecchio, R. D. (2002). Chromophoric DOM in the coastal environment. In D. A. Hansell, & C. A. Carlson (Eds.), *Biogeochemistry of Marine Dissolved Organic Matter* (pp. 509–546).

Bowers, D. G., Harker, G. E. L., & Stephan, B. (1996). Absorption spectra of inorganic particles in the Irish Sea and their relevance to remote sensing of chlorophyll. *International Journal of Remote Sensing*, *17*, 2449–2460.

Bricaud, A., Morel, A., & Prieur, L. (1981). Absorption by dissolved organic matter of the sea (yellow Substance) in the UV and visible domains. *Limnology and Oceanography*, *26*, 43–53.

Carder, K. L., Chen, F. R., Lee, Z. P., Hawes, S. K., & Kamykowski, D. (1999). Semianalytic Moderate-Resolution Imaging Spectrometer algorithms for chlorophyll a and absorption with bio-optical domains based on nitrate-depletion temperatures. *Journal of Geophysical Research*, *104*, 5403–5421.

Chen, Y. L. L., Chen, H. Y., Lin, I. I., Lee, M. A., & Chang, J. (2007). Effects of cold eddy on phytoplankton production and assemblages in Luzon Strait bordering the South China Sea. *Journal of Oceanography*, *63*, 671–683.

Coble, P. G. (2007). Marine optical biogeochemistry: The chemistry of ocean color. *Chemical Reviews-Columbus*, *107*, 402–418.

Dai, M., Zhai, W., Cai, W., Callahan, J., Huang, B., Shang, S., Huang, T., Li, X., Lu, Z., Chen, W., & Chen, Z. (2008). Effects of an estuarine plume-associated bloom on the carbonate system in the lower reaches of the Pearl River estuary and the coastal zone of the northern South China Sea. *Continental Shelf Research*, *28*, 1416–1423.

Dong, Q. (2010). *Derivation of Phytoplankton Absorption Properties from Ocean Color and Its Application*. PhD Thesis, Xiamen University, Xiamen, China.

Dong, Q., Hong, H., & Shang, S. (2008). A new approach to correct for pathlength amplification in measurements of particulate spectral absorption by the quantitative filter technique. *Journal of Xiamen University (Natural Science)*, *47*, 556–561.

Dong, Q., Hong, H., & Shang, S. (2009). Differences between two methods for particle absorption measurements in case-2 waters. *Journal of Xiamen University (Natural Science)*, *48*, 293–297.

Du, C., Shang, S., Dong, Q., Hu, C., & Wu, J. (2010). Characteristics of chromophoric dissolved organic matter in the nearshore waters of the western Taiwan Strait. *Estuarine, Coastal and Shelf Science*, *88*, 350–356.

Gan, J., Li, L., Wang, D., & Guo, X. (2009). Interaction of a river plume with coastal upwelling in the northeastern South China Sea. *Continental Shelf Research*, *29*, 728–740.

Gordon, H. R., & Wang, M. (1994). Retrieval of water-leaving radiance and aerosol optical thickness over the oceans with SeaWiFS: A preliminary algorithm. *Applied Optics*, *33*, 443–452.

Green, S. A., & Blough, N. V. (1994). Optical absorption and fluorescence properties of chromophoric dissolved organic matter in natural waters. *Limnology and Oceanography*, *39*, 1903–1916.

Hong, H., Wu, J., Shang, S., & Hu, C. (2005). Absorption and fluorescence of chromophoric dissolved organic matter in the Pearl River Estuary, South China. *Marine Chemistry*, *97*, 78–89.

Hong, H., Zhang, C., Shang, S., Huang, B., Li, Y., Li, X., & Zhang, S. (2009). Interannual variability of summer coastal upwelling in the Taiwan Strait. *Continental Shelf Research*, *29*, 479–484.

International Ocean-Colour Coordinating Group (IOCCG) (2006). Remote sensing of inherent optical properties: Fundamentals, tests of algorithms, and applications. In Z. P. Lee (Ed.), *Reports of the International Ocean-Colour Coordinating Group, No. 5*. Dartmouth, Canada: IOCCG.

Jan, S., Wang, J., Chern, C. S., & Chao, S. Y. (2002). Seasonal variation of the circulation in the Taiwan Strait. *Journal of Marine Systems*, *35*, 249–268.

Jerlov, N. G. (1968). *Optical Oceanography*. New Youk: Elsevier.

Karentz, D., & Lutze, L. H. (1990). Evaluation of biologically harmful ultraviolet radiation in Antarctica with a biological dosimeter designed for aquatic environments. *Limnology and Oceanography*, *35*, 549–561.

Kiefer, D. A., & SooHoo, J. B. (1982). Spectral absorption by marine particles of coastal waters of Baja California. *Limnology and Oceanography*, 492–499.

Kishino, M., Takahashi, M., Okami, N., & Ichimura, S. (1985). Estimation of the spectral absorption coefficients of phytoplankton in a thermally stratified sea. *Bulletin of Marine Science*, *37*, 634–642.

Lee, Z. (1994). *Visible-infrared Remote-sensing Model and Applications for Ocean Waters*. PhD Thesis, University of South Florida, St. Petersburg, Florida.

Lee, Z., Ahn, Y. -H., Mobley, C., & Arnone, R. (2010). Removal of surface-reflected light for the measurement of remote-sensing reflectance from an above-surface platform. *Optics Express*, *18*, 26313–26342.

Lee, Z., Carder, K. L., & Arnone, R. A. (2002). Deriving inherent optical properties from water color: A multiband quasi-analytical algorithm for optically deep waters. *Applied Optics*, *41*, 5755–5772.

Lee, Z., Lubac, B., Werdell, J., & Arnone, R. (2009). An Update of the Quasi-Analytical Algorithm (QAA_v5). http://www.ioccg.org/groups/Software_OCA/QAA_v5.pdf

Liu, K. K., Chao, S. Y., Shaw, P. T., Gong, G. C., Chen, C. C., & Tang, T. (2002). Monsoon-forced chlorophyll distribution and primary production in the South China Sea: Observations and a numerical study. *Deep Sea Research Part I: Oceanographic Research Papers*, *49*, 1387–1412.

Lohrenz, S. E., & Cai, W. J. (2006). Satellite ocean color assessment of air–sea fluxes of CO_2 in a river-dominated coastal margin. *Geophysical Research Letters*, *33*, L01601.

Mannino, A., Russ, M. E., & Hooker, S. B. (2008). Algorithm development and validation for satellite-derived distributions of DOC and CDOM in the US Middle Atlantic Bight. *Journal of Geophysical Research*, *113*, http://dx.doi.org/10.1029/2007JC004493.

Matsuoka, A., Huot, Y., Shimada, K., Saitoh, S. I., & Babin, M. (2007). Bio-optical characteristics of the western Arctic Ocean: Implications for ocean color algorithms. *Canadian Journal of Remote Sensing*, *33*, 503–518.

Mélin, F., Zibordi, G., & Berthon, J. F. (2007). Assessment of satellite ocean color products at a coastal site. *Remote Sensing of Environment*, *110*, 192–215.

Mitchell, B. G., Bricaud, A., & Carder, K. (2000). Determination of spectral absorption coefficients of particles, dissolved material and phytoplankton for discrete water samples. In G. S. Fargion, & J. L. Mueller (Eds.), *Ocean Optics Protocols For Satellite Ocean Color Sensor Validation, Revision 2* (pp. 125–153). Greenbelt, Maryland: NASA Goddard Space Flight Space Center.

Morel, A. (2009). Are the empirical relationships describing the bio-optical properties of case 1 waters consistent and internally compatible? *Journal of Geophysical Research*, *114*, http://dx.doi.org/10.1029/2008JC004803.

Nelson, N., Siegel, D., & Michaels, A. (1998). Seasonal dynamics of colored dissolved material in the Sargasso Sea. *Deep-Sea Research Part I*, *45*, 931–957.

Roesler, C. S., Perry, M. J., & Carder, K. L. (1989). Modeling in situ phytoplankton absorption from total absorption spectra in productive inland marine waters. *Limnology and Oceanography*, *34*, 1510–1523.

Shang, S., Li, L., Li, J., Li, Y., Lin, G., & Sun, J. (2012). Phytoplankton bloom during the northeast monsoon in the Luzon Strait bordering the Kuroshio. *Remote Sensing of Environment*, *124*, 38–48.

Siegel, D. A., Maritorena, S., Nelson, N. B., Hansell, D. A., & Lorenzi-Kayser, M. (2002). Global distribution and dynamics of colored dissolved and detrital organic materials. *Journal of Geophysical Research-Oceans*, *107*, 3228, http://dx.doi.org/10.1029/2001JC000965.

Tassan, S., & Ferrari, G. M. (1995). An alternative approach to absorption measurements of aquatic particles retained on filters. *Limnology and Oceanography*, *40*, 1358–1368.

Tzortziou, M., Subramaniam, A., Herman, J. R., Gallegos, C. L., Neale, P. J., & Harding, L. W. (2007). Remote sensing reflectance and inherent optical properties in the mid Chesapeake Bay. *Estuarine, Coastal and Shelf Science*, *72*, 16–32.

Vodacek, A., Blough, N., DeGrandpre, M., Peltzer, E., & Nelson, R. (1997). Seasonal variation of CDOM and DOC in the Middle Atlantic Bight: Terrestrial inputs and photooxidation. *Limnology and Oceanography*, *42*, 674–686.

Wang, W., Dong, Q., Shang, S., Wu, J., & Lee, Z. (2009). An evaluation of two semi-analytical ocean color algorithms for waters of the South China Sea. *Journal of Tropical Oceanography (Chinese)*, *28*, 35–42.

Werdell, P. J., & Bailey, S. W. (2005). An improved in-situ bio-optical data set for ocean color algorithm development and satellite data product validation. *Remote Sensing of Environment*, *98*, 122–140.

Zhu, W., Yu, Q., Tian, Y. Q., Chen, R. F., & Gardner, G. B. (2011). Estimation of chromophoric dissolved organic matter in the Mississippi and Atchafalaya river plume regions using above-surface hyperspectral remote sensing. *Journal of Geophysical Research*, *116*, http://dx.doi.org/10.1029/2010JC006523.